AIAA JOURNAL
Vol. 34, No. 11, November 1996

Algebraic Turbulence Model Simulations of Supersonic Open-Cavity Flow Physics

Chung-Jen Tam,* Paul D. Orkwis,† and Peter J. Disimile‡
University of Cincinnati, Cincinnati, Ohio 45221-0070

A time-accurate double thin-layer Navier–Stokes computation is performed for an unsteady supersonic open cavity with a length-to-depth ratio of 2. The results are used to determine the flow-physics mechanisms responsible for the cavity oscillation cycle. A new cycle is described and compared to previous descriptions. It is found that a shed vortex impinges on the cavity aft lip and forms a pressure pulse that augments or forces, at the vortex shedding frequency, an internal upstream moving wave that has been reflected from the aft corner. This upstream moving wave eventually reflects off the cavity forward wall and forces the shedding of a new vortex. It was found, however, that the reflected wave dissipates before it reaches the aft wall. Instead, a second wave forms beneath the shed vortex and eventually reflects from the aft corner and is forced at the shedding frequency by the shed vortex wave, completing the cycle.

Introduction

THE basic physical structure of cavity flowfields can be described as either closed, open, or transitional.[1–4] Closed cavities are typically long and shallow with a length-to-depth ratio (L/D) greater than 13. These are characterized by a shear layer that impinges on the cavity floor, producing two large recirculation regions. Closed cavities are associated with higher drag coefficients[5–8] and heat transfer properties[9–11] than those of open cavities; as such, they are less desirable. Open cavities are short and deep with an $L/D < 10$. They contain shear layers that span the cavity and are more typical of those found in aircraft applications. Open-cavity flowfields are remarkably complicated, with internal and external regions that are coupled via self-sustained shear-layer oscillations. Coherent shed vorticity, unsteady weak shock or pressure waves, and interactions between the shed vortices and the vortices that reside in the cavity also are present. Flowfield characteristics appear to depend primarily on the shape of the cavity and the Mach number, with Reynolds number effects considered to be less important.[12,13]

Several issues remain to be understood for open-cavity flowfields. Researchers appear to agree that an oscillating shear layer exists, that the primary and secondary vortices residing within the cavity are driven by the shear layer, that a mass breathing effect occurs within the cavity, and that pressure oscillations exist. However, the mechanisms driving this flowfield have not yet been agreed upon.

Because of the unsteady nature of supersonic open-cavity flowfields, the measurement of field properties within the cavity is difficult experimentally. As such, surface properties, such as time-averaged pressure and time-averaged sound-pressure level (SPL), are usually reported in the literature. Unsteady quantities typically are presented in terms of the spectral SPL. Recent experimental work[12] for subsonic to transonic open cavities provides a benchmark for comparing the effects of different Mach numbers, aspect ratios, flowfield dimensionality (i.e., two- and three-dimensional), and surface heating. However, no field data were reported to enable an examination of the pressure oscillation driving mechanisms. This is not uncommon because few experimental works have provided flow visualization about supersonic open cavities. In spite of this, experimental efforts have contributed useful information about the pressure oscillation cycle mechanisms. Prominent works have attempted to describe the details of open-cavity flowfields.[13–15] Their proposed physical mechanisms are discussed in detail in the following section.

Numerical results have produced considerable evidence regarding the nature of the cavity resonance cycle. A number of researchers have attempted to simulate the open-cavity resonance cycle.[16–23] All of these efforts employed a Reynolds-averaged Navier–Stokes equation approach with an algebraic turbulence model. More advanced turbulence models, such as one-equation[24] and two-equation[25] models, also have been attempted, although with no greater success. The general results indicate that a variety of solutions can be obtained with the various turbulence models, but that the large-scale features are similar for the best performing models. Good results are typically obtained for time-averaged surface properties such as pressure and shear stress. However, unsteady properties such as SPLs and cavity resonance frequencies are not computed consistently. This is not surprising because turbulence models are typically not tuned to unsteady applications.

Apart from computing the unsteady cavity flowfield, experimental and computational studies of cavities with suppression devices have been performed by many researchers. Sarno and Franke[26] studied the effects of manipulating the shear layer over the cavity leading edge by using static and oscillating fences as well as steady- and pulsating-flow injection at the leading edge of the cavity. Pereira and Sousa[27] measured the time-averaged velocity flowfield and turbulent velocity characteristics of different cavity trailing-edge geometries (sharp, nose-shape, and round) using laser Doppler anemometry. Baysal et al.[28] performed computational simulations for the two-dimensional transonic turbulent flows past a cavity with a rear face ramp and then with a spoiler at the front lip. Kim and Chokani[29] conducted a computational investigation to study the effect of passive control on a supersonic flow over a two-dimensional cavity. The passive control was implemented by using a porous surface over a vent chamber in the cavity floor. Jeng and Payne[30] further computed the effect of porous walls, separately placed at the forward bulkhead, floor, and aft bulkhead, to suppress the pressure fluctuations within the cavity. Suhs[19] used an implicit Navier–Stokes code with a thin-layer approximation to compute the flow over a three-dimensional rectangular cavity with and without a solid spoiler at the leading-edge lip. All of these results show the effect of passive controls on the pressure oscillations in the cavities. However, few details of the unsteady field properties were reported to help explain the inherent flow physics.

Understanding of the flowfield in the cavity can help to determine the driving mechanisms for the cavity oscillation cycle and can be

Presented as Paper 96-0075 at the AIAA 34th Aerospace Sciences Meeting, Reno, NV, Jan. 15–18, 1996; received Feb. 12, 1996; revision received June 18, 1996; accepted for publication June 25, 1996; also published in *AIAA Journal on Disc*, Volume 2, Number 1. Copyright © 1996 by the authors. Published by the American Institute of Aeronautics and Astronautics, Inc., with permission.

*Research Assistant. Member AIAA.
†Assistant Professor, Department of Aerospace Engineering and Engineering Mechanics. Senior Member AIAA.
‡Associate Professor, Department of Aerospace Engineering and Engineering Mechanics. Member AIAA.

used to create an effective method to suppress the undesired resonance frequencies and to avoid structural damage. Computational fluid dynamics is uniquely able to visualize this highly unsteady flowfield and to illustrate time histories of flow properties that can be used to better understand the physical mechanisms leading to the oscillation cycle.

The main goal of the current research was to determine the flow-physics mechanisms about the supersonic two-dimensional open cavity (defined earlier) that are responsible for the resonance cycle. A numerical method was applied that uses the double thin-layer Navier–Stokes (DTLNS) equations and a modified version of the Baldwin–Lomax algebraic turbulence model applied previously,[28] which has been compared with the experimental data of Disimile and Orkwis.[31] The following sections discuss the numerical scheme; the physical mechanisms associated with supersonic two-dimensional open cavities proposed by Heller and Bliss[14] and mentioned by Rockwell and Naudascher[15]; the results obtained in the current research, including a new description of the cavity oscillation mechanism and a discussion of the similarities and differences between the new cycle and those mentioned above; and the conclusions drawn from this study.

Numerical Scheme

The equations solved discretely in the current work are the DTLNS equations. The multiblock finite volume scheme developed by Simpson and Whitfield[32] and modified by Tam et al.[23] was used. The current procedure was detailed in earlier works[22,23] and are not included in the present discussion. The scheme utilizes Roe flux difference splitting for the residual and an approximate Steger–Warming splitting for the Jacobian matrix. It is third-order accurate in space and second-order accurate in time when a Newton-like subiteration procedure is employed.[32] Four subiterations per global iteration were used, in the manner of Simpson and Whitfield,[32] because this reduces the subiteration residual sufficiently to attain second-order temporal accuracy.

In an earlier work,[23] several different modifications of the Baldwin–Lomax turbulence model and a laminar calculation were tested for application to supersonic two-dimensional open-cavity flowfields. The results showed that an increase in eddy viscosity caused the flowfield solution to be more dissipative, and that highly dissipative models, such as the standard Baldwin–Lomax model, underpredicted the dominant frequencies and the overall SPLs. The laminar case (without the eddy viscosity) had the opposite effect on the surface-property predictions. The authors later found that the version of the Baldwin–Lomax model employed previously by Baysal et al.,[28] which was modified to employ upstream relaxation,[33,34] multiple walls,[25,28] and the first peak modification,[35,36] had the best overall predictions as compared to experimental data[31] based on time-averaged surface pressure, time-averaged SPL, dominant frequencies, and SPL vs frequency.

These modifications of the Baldwin–Lomax turbulence model were used to account for both the flow features and the cavity geometry. For example, the relaxation modification was implemented to eliminate the abrupt change in eddy viscosity from the flat-plate boundary layer to the free shear layer at the mouth of the cavity. The multiple-wall modification was used to include the effects of all cavity walls on the computed eddy viscosity. For separated flows, such as in the open cavity, the function $F(y)$ has multiple peaks. The first peak modification chooses the F function peak nearest the wall. The details of these modifications were discussed previously[23] and, for brevity, are omitted here.

Boundary and Initial Conditions

Boundary conditions for the computation were prescribed variables on the inflow plane, no-slip adiabatic wall on solid surfaces, and extrapolation on the outflow boundaries. The upstream profile was determined by using a flat-plate computation from which the proper profile was chosen by finding the x location with the same momentum thickness as that found experimentally.[22]

Initial conditions for the flowfield external to the cavity were obtained by extrapolating the inflow profile, i.e., a constant boundary-layer profile was set along the flat plates and above the cavity. Flow inside the cavity was initialized by using the wall pressure and density of the flat plate. The nondimensional velocity components were prescribed via the equations $\rho u = 0.5$, $\rho v = \rho w = 0.0$, which represented a slow uniform flow in the x direction inside the cavity. The total energy then was defined from these quantities. Note that these are arbitrary settings for the flow conditions inside the cavity.

Grids

The block-grid dimensions for this study were 66×55, 66×120, and 66×55 for the upstream, cavity, and downstream blocks, respectively, with points clustered along all walls. This choice was based on a grid-resolution study, the results of previous researchers, and available computational resources. Half and double x- and y-direction grid-point densities were tested, and the fine-grid results were only marginally different.

Data Sampling

The results were obtained over a period of 71 characteristic times t_c. The total run time was approximately 212 h on a Cray 90 supercomputer. Data were sampled after $6t_c$, as per the suggestion of Suhs,[19] which allowed the initial starting transient to decay. A sampling rate of 4.292×10^{-9} s, which corresponded to a nondimensional time step of 1×10^{-4}, was employed for surface pressure, whereas 8.584×10^{-7} s was used to sample the field properties for the entire flow.

Physical-Mechanism Theories

The code as described above was employed to explore the validity of the flow-physics mechanisms described previously by experimental investigations. Notable efforts by Rossiter,[13] Heller and Bliss,[14] and Rockwell and Naudascher[15] have attempted to describe the details of open-cavity flowfields. Surprisingly, the general descriptions are, at first glance, quite different but can be reinterpreted as different perspectives on the same events.

Rossiter's Empirical Formula

Rossiter employed dimensional analysis and empiricism to produce the following formula for the cavity resonance frequencies:

$$f = \frac{U}{L} \frac{(m - \gamma)}{[(1/K) + M]} \tag{1}$$

where U is the freestream velocity, L is the cavity length, M is the Mach number, m is an integer $(1, 2, 3, \ldots)$, and $\gamma = 0.25$ and $K = 0.66$ are constants. Note again that Rossiter's formula does not contain a Reynolds number. Rossiter's formula predicts the dominant frequency of the cavity oscillation with remarkable accuracy, as demonstrated previously.[23] This value can be obtained from numerical simulations and is one of the more appropriated accuracy metrics for this unsteady flow.

Rossiter's model was derived using an edge-tone analogy and the assumption that the acoustic radiation is attributable to shed vortices impinging on the cavity aft wall. His experiments visualized the shed vortices and the pressure waves external to the cavity, although they did not visualize the standing waves described as existing within the cavity. This work laid the foundation for the more comprehensive theories regarding cavity resonance put forth by Heller and Bliss[14] and Rockwell and Naudascher.[15]

Heller-Bliss Wave Interaction Mechanism

The mechanism proposed by Heller and Bliss[14] and cited by several other researchers[17,20] defines the shear-layer oscillation cycle as dependent on unsteady planar compression waves. The upstream traveling compression wave reaches the front wall, reflects back, and becomes a downstream traveling wave. The resulting wave pattern in the cavity causes unsteadiness in the shear layer. In turn, the shear-layer motion is responsible for the aft wall mass addition and removal that initially generates the cavity internal wave structure. Figure 1 shows the process of the feedback loop in the cavity, as follows.

1) The pressure wave from a previous trailing-edge disturbance reaches the front wall of the cavity and reflects. Another wave, which has already reflected off the front wall, approaches the aft wall of

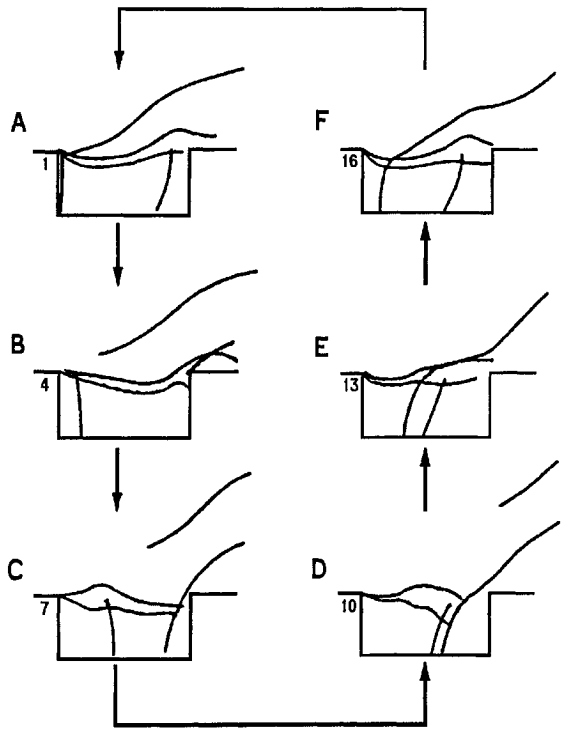

Fig. 1 Typical oscillation cycle.

the cavity. At this time, the shear layer is deflected above the aft wall, and fluid leaves the cavity near the aft end.

2) The shear-layer oscillation travels downstream in a wave-like pattern and eventually hits the trailing edge. A new compression wave begins to form at the aft wall as the flow impinges on the trailing edge, causing fluid to enter the cavity. The compression wave reflected from the front wall travels downstream approximately in phase with the shear-layer displacement.

3) The shear layer, which is now below the trailing edge at the aft wall, forms an upstream traveling compression wave. The reflected wave from the front wall continues to move downstream in phase with the shear-layer displacement.

4) The upstream and downstream compression waves meet and interact near the cavity center.

5) After interaction, the waves continue in their respective directions. The external part of the upstream traveling wave moves into the supersonic flow, thus causing it to be tipped more than the external-flow Mach angle. The downstream wave moves in the same direction as the external flow and travels at a subsonic speed relative to it. At the aft wall, the shear layer reaches the trailing-edge height.

6) The shear layer is now above the trailing edge. The wave generated at the trailing edge approaches the front wall of the cavity, and the downstream traveling wave approaches the aft wall of the cavity. The oscillation cycle then repeats.

Vortex Interaction Mechanism

Rockwell and Naudascher[15] and others[37,38] provide an explanation of the cavity resonance cycle, which stipulates that the shear-layer oscillation is driven primarily by transient vortex motions within the cavity. They contend that the vortices that form within the oscillating shear layer sometimes impinge upon the aft wall and then mix with vortices inside the cavity. The shear-layer vortex/edge interaction adds mass to the cavity, the breathing-in phase. This captured vortex then interacts with the internal cavity vortices, displacing them and producing pressure oscillations within the cavity. These fluctuations travel forward and eventually displace the shear layer at the leading edge. This produces an external excitation of the shear layer that initiates and locks in the shedding of another vortex and closes the feedback loop.

Note that although the two descriptions appear to be quite different, the two points of view are not mutually exclusive. The following section discusses the results from the present calculation, compares them with the two physical oscillation mechanisms mentioned above, and describes a new oscillation-cycle mechanism.

Results and Discussion

The results include a comparison of the dominant frequency with the Rossiter formula prediction and time histories of simulated schlieren images and vorticity and pressure contours for one oscillation cycle. The schlieren simulation was produced to numerically create pressure-wave images and compare them with the Heller and Bliss[14] experimental results. Results were obtained to match the experimental data taken previously[31] for flow about an $L/D = 2$ quasi-two-dimensional cavity in terms of dominant frequency and time-averaged SPLs. The test parameters were $M_\infty = 2$, $Re_\theta = 3.69 \times 10^4$, and $\theta = 0.979$ mm. No flow visualization was available from the experiment.

Dominant Frequency

The time history of pressure was taken along the wall surfaces after every iteration of the computation. There were 325,000 data points for each wall grid point. A fast Fourier transform (FFT) was used to decompose the pressure signal along the cavity walls, i.e., the front wall, the floor, and the aft wall. The resulting FFT showed that the dominant frequencies were the same throughout the cavity, with a value of 26.2 kHz and a time-averaged SPL ($\overline{\text{SPL}}$) of 167.54 dB at the $x/L = \frac{2}{3}$ point on the cavity floor. These numbers should be compared with the dominant frequency described by Rossiter's formula [Eq. (1)] and the $\overline{\text{SPL}}$ value found from the experiment.[31] Rossiter's formula predicts frequencies of $f = 9916$, 23,138, and 36,360 Hz for the first three modes, respectively. Rossiter notes that the dominant peak is one of these values, although not necessarily the first. The current numerical result agrees quite well with the second mode, and also with the experimental measurements of approximately 23 kHz and 164.41 dB. Note that many other algebraic turbulence models were tested previously by the authors.[23] These other results provided reasonable agreement with the dominant frequency, but poor agreement with the $\overline{\text{SPL}}$. This is noteworthy, considering that $\overline{\text{SPL}}$ is measured on a decibel scale. For these reasons, the above comparisons provide some confidence in the computed solution.

Combined-Schlieren Simulation and Vorticity Contours

The pressure fluctuations in the cavity were reported by Heller and Bliss[14] using water-table visualization. Density variations in the flowfield can be observed with that technique. The numerical results were used to obtain a combined-schlieren simulation of the pressure-wave structure in the cavity, i.e., magnitude of the density gradient:

$$|\nabla\rho| = \sqrt{\left(\frac{\partial\rho}{\partial x}\right)^2 + \left(\frac{\partial\rho}{\partial y}\right)^2} \tag{2}$$

(Note that experimental schlieren images have a preferred direction, i.e., they are either $\partial\rho/\partial x$ or $\partial\rho/\partial y$, depending on the orientation of the knife edge. The current combined simulation then is a merging of results taken with both knife-edge orientations.)

The resulting pressure-wave patterns can be used to determine the feedback mechanism for the oscillation cycle in the cavity, as shown in Fig. 2. All of the cycle time histories were divided into eight time-sequential events that form a continuous loop. Figure 3 is an enhanced sketch of the original combined-schlieren simulation. This diagram was produced by importing the original plot (Fig. 2) into Microsoft Windows PaintBrush and highlighting the main features of the pressure waves. The wave patterns are labeled a, b, c, and v (their explanation is provided below). The prime indicates the wave generated from the previous oscillation cycle and the asterisk represents the beginning-wave pattern for the next cycle. A starting point for the cycle is arbitrarily chosen, because it is necessary to review the entire process to completely understand the conditions throughout.

Observed Oscillation Cycle

The oscillation cycle observed in the numerical simulations can be described as follows:

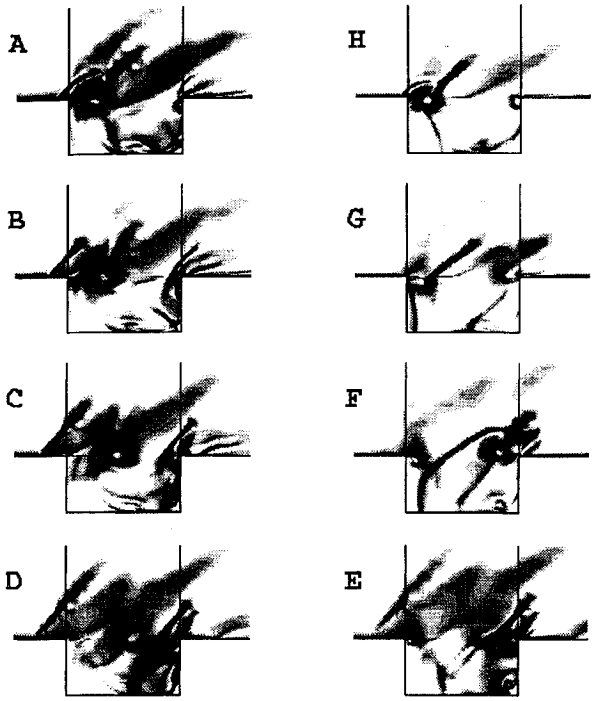

Fig. 2 Time history of schlieren simulation.

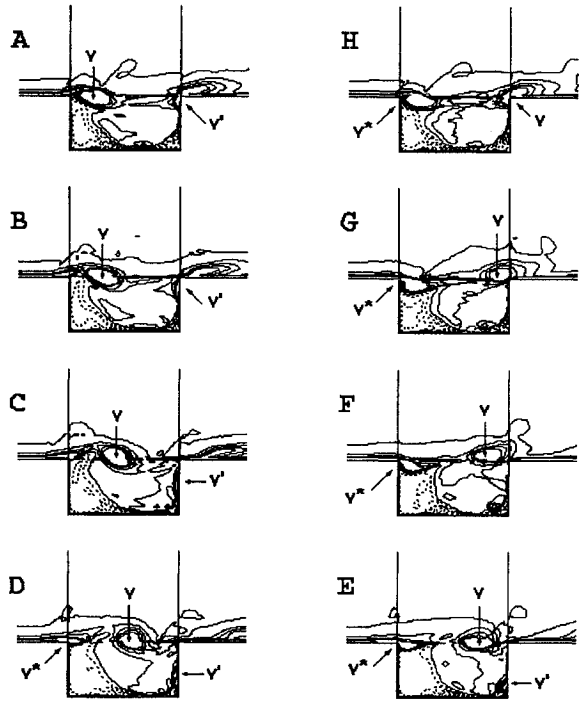

Fig. 4 Time history of vorticity contour.

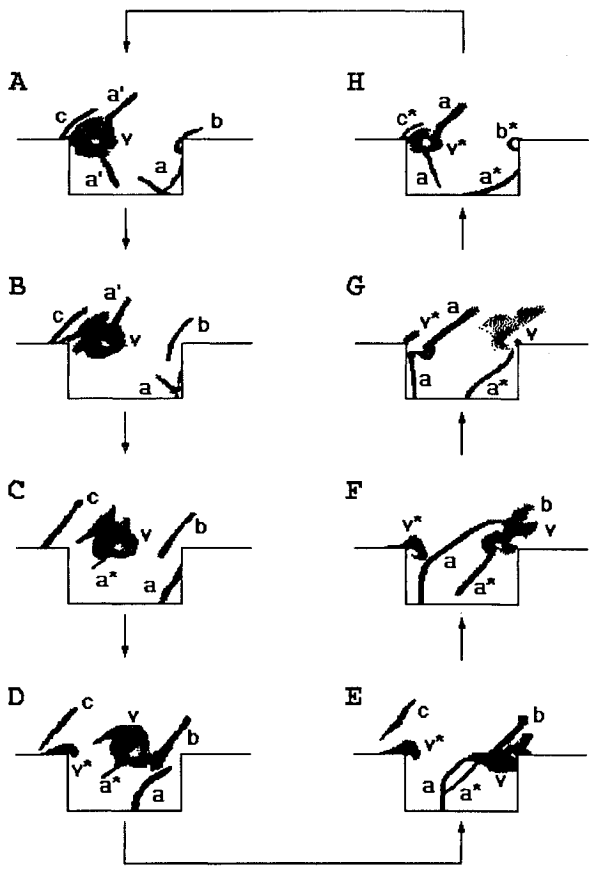

Fig. 3 Enhanced sketch of schlieren simulation.

1) A downstream moving compression wave a' has been reflected from the front wall. This reflection creates a compression wave c that travels upstream of the separation lip, a second downstream moving compression wave a approaches the aft-wall corner and is reflecting off the cavity floor. At this point, note that although a' had previously reflected from the forward and aft walls (much like wave a is preparing to do in the current cycle), wave a did not form from a wave like a'. This is fundamentally different from the Heller–Bliss cycle and is discussed further below. At the trailing-edge cavity lip, a compression wave b is formed because of the impingement and shredding of the shed vortex v' (Fig. 4A), whereas another vortex v is in the formation process at the leading edge.

2) The internal portion of the downstream traveling compression wave a' has been dissipated and does not propagate farther downstream. Meanwhile, the aft compression wave a impinges on the cavity floor and begins reflecting from the corner, demonstrating that a was not formed by the reflection of a' from the front wall.

The pressure wave at the trailing-edge lip b travels upstream a bit, but then remains quite stationary. At the same time, the shed vortex v' is torn into two parts at the trailing-edge lip; one is convected downstream and the other moves into the cavity as shown in Fig. 4B. The leading-edge vortex v continues the shedding process caused by the high pressure (Fig. 5B) induced by the reflection of a'.

3) A compression wave a^* starts to form just beneath the vortex and travels downstream. This is the wave that eventually will strike the aft-wall corner (like wave a in Fig. 3A). It represents a major difference with the Heller and Bliss cycle.

Near the forward wall, the high pressure in the separation-lip region (Fig. 5C) continues to push the vortex v upward as it sheds. In the bottom right corner, wave a reflects and moves upstream. The torn vortex v' travels downward (Fig. 4C) and provides an additional forcing influence on wave a as it moves away from the aft wall. Note that, unlike the Heller–Bliss[14] and Rockwell–Naudascher[15] descriptions, the impinging vortex does not form the upstream traveling wave. Rather, it appears to augment or force the wave at the vortex-shedding frequency. This is likely the feedback mechanism needed to attain the consistent oscillatory behavior seen in the cavity. The nonlinear nature of this forcing also provides an explanation for why the cycle is somewhat irregular, even though a dominant frequency can be determined.

4) The internal compression waves a and a^* travel in their respective directions. The torn vortex v' moves farther downward in the cavity and mixes with the resident vortex (Fig. 4D). By this time, the shed vortex v has detached from the separation lip and begins to convect downstream, while a small portion of the next vortex v^* begins the formation process.

5) Inside the cavity, the upstream traveling compression wave a interacts with the downstream compression wave a^*; they then continue in their respective directions. However, wave a now becomes more of a normal shock. The shed vortex v reaches the trailing-edge

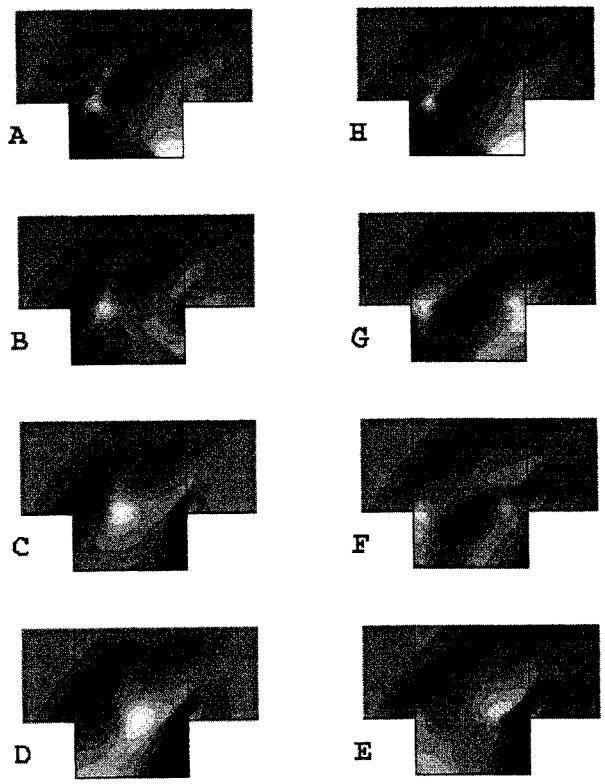

Fig. 5 Time history of pressure contour.

lip, as shown in Fig. 4E, while at the leading edge, the next vortex v^* continues to form.

6) The compression wave a propagates upstream like a normal shock inside the cavity and approaches the forward wall, while forming an oblique shock outside the cavity. The downstream traveling compression wave a^* moves toward the lower aft-wall corner. Figure 4F shows that the shed vortex v contacts the trailing-edge lip.

7) The internal portion of the upstream traveling pressure wave a reflects off the front wall and begins to move downstream. The external portion essentially stalls when it meets the shedding vortex v^*. The pressure wave b dissipates at the trailing-edge lip, at the same time, the shed vortex v impinges on the trailing-edge lip (Fig. 4G).

8) The impingement of the pressure wave at the separation lip forms an upstream traveling compression wave c^* forward of the separation lip. Compression wave a convects farther downstream. At the aft-wall corner, compression wave a^* impinges on the cavity floor and the aft wall. At the same time, the shed vortex impinges on the trailing-edge lip and creates a compression wave b^*, again indicating that the mechanism that creates the upstream traveling wave comes first (because of the downstream traveling-wave reflection), preceding the generation of the pressure pulse from the vortex impingement. The next cycle starts with A, and the oscillation in the cavity repeats.

The current results indicate that the pressure oscillation in the supersonic two-dimensional open cavity is generated by the impingement of compression waves on the bottom aft wall. This wave is not formed by the impinging vortex but rather is forced by that vortex in the same manner as a forced pendulum. This wave later reflects off the aft wall and travels upstream, thus forcing another vortex to shed at the leading-edge lip and initiating the next cycle. However, this pressure wave eventually dissipates near the center of the cavity and a new pressure wave forms below the shed vortex that travels downstream and continues the cycle.

Cycle Differences

Note that there are some differences between the present pressure oscillation mechanism and those proposed by Heller and Bliss[14] and Rockwell and Naudascher.[15] In particular, note the following.

1) The compression wave formed at the bottom aft corner starts not from the previous cycle wave but from the wave just below the shed vortex, as shown in Fig. 3C.

2) The downstream traveling-compression wave that had reflected off the front wall dissipates near the center of the cavity (Figs. 3A–3C) and does not strike the aft wall.

3) The upstream traveling compression wave does not have a component outside the cavity until it interacts with the downstream traveling compression wave (Fig. 3F), at which point it picks up the downstream lip compression wave.

4) Although the shed vortex and the vortex impingement are observed from the numerical results, little evidence exists to suggest that the torn vortex entering the cavity is responsible for the pressure oscillation mechanism as suggested by Rockwell and Naudascher.[15] Rather, it appears to provide a forcing function for the pressure wave.

Conclusions

A study of the flow physics about a supersonic two-dimensional open cavity has been performed using a time-accurate DTLNS equation flow solver. A combined-schlieren simulation, vorticity, and pressure contours were used to show that a shed vortex impinges on the cavity aft lip and forms a pressure pulse that augments or forces, at the vortex shedding frequency, an internal upstream moving wave that has been reflected from the aft lower corner. This upstream moving wave eventually reflects off the cavity forward wall and forces the shedding of a new vortex. However, it was found that the reflected wave dissipates before it reaches the aft wall. Instead, a second wave forms beneath the shed vortex and eventually reflects from the aft corner and is forced at the shedding frequency by the shed vortex wave, completing the cycle.

Acknowledgments

This research was funded in part by Leonidas Sakell and the U.S. Air Force Office of Scientific Research through Grant F49620-93-0081 and by the Ohio Aerospace Institute and G.E. Aircraft Engines through Core Collaborative Research Program Grant 94-2-018. Additional computational resources were provided by the U.S. Army Waterways Experimental Shared Resource Center through Dave Belk of the U.S. Air Force Wright Laboratory at Eglin Air Force Base.

References

[1]Roshko, A., "Some Measurements of Flow in a Rectangular Cutout," NACA TN 3488, Aug. 1955.

[2]McDearmon, R. W., "Investigation of the Flow in a Rectangular Cavity in a Flat Plate at a Mach Number of 3.55," NASA TN D-523, Sept. 1960.

[3]Tracy, M. B., Plentovich, E. B., and Chu, J., "Measurements of Fluctuating Pressure in a Rectangular Cavity in Transonic Flow at High Reynolds Numbers," NASA TM 4363, June 1992.

[4]Tracy, M. B., and Plentovich, E. B., "Characterization of Cavity Flow Fields Using Pressure Data Obtained in the Langley 0.3-Meter Transonic Cryogenic Tunnel," NASA TM 4436, March 1993.

[5]Charwat, A. F., Roos, J. N., Dewey, C. F., and Hitz, J. A., "An Investigation of Separated Flows, Part 1: The Pressure Field," *Journal of the Aerospace Sciences*, Vol. 28, No. 6, 1961, pp. 457–470; "An Investigation of Separated Flows, Part 2: Flow Separation in the Cavity and Heat Transfer," *Journal of the Aerospace Sciences*, Vol. 28, No. 7, 1961, pp. 513–527.

[6]McGregor, O. W., and White, R. A., "Drag of Rectangular Cavities in Supersonic and Transonic Flow Including the Effect of Cavity Resonance," *AIAA Journal*, Vol. 8, No. 11, 1970, pp. 1959–1964.

[7]Catani, U., Bertin, J. J., DeAmicis, R., Masullo, S., and Bouslog, S. A., "Aerodynamic Characteristics for a Slender Missile with Wrap-Around Fins," *Journal of Spacecraft and Rockets*, Vol. 20, No. 2, 1983, pp. 122–128.

[8]Blair, A. B., Jr., and Stallings, R. L., Jr., "Supersonic Axial Force Characteristics of a Rectangular Box Cavity with Various Length-to-Depth Ratios in a Flat Plate," NASA TM-87659, April 1986.

[9]Hahn, M., "Experimental Investigation of Separated Flow over a Cavity at Hypersonic Speed," *AIAA Journal*, Vol. 7, No. 6, 1969, pp. 1092–1098.

[10]Nestler, D. E., Saydah, A. R., and Auxler, W. L., "Heat Transfer to Steps and Cavities in Hypersonic Turbulent Flow," *AIAA Journal*, Vol. 7, No. 7, 1969, pp. 1368–1370.

[11]Nestler, D. E., "An Experimental Study of Hypersonic Cavity Flow," *Journal of Spacecraft and Rockets*, Vol. 19, No. 3, 1982, pp. 195, 196.

[12]Ahuja, K. K., and Mendoza, J., "Effects of Cavity Dimensions, Boundary Layer, and Temperature on Cavity Noise with Emphasis on Benchmark Data to Validate Computational Aeroacoustic Codes," NASA CR 4653, April 1995.

[13]Rossiter, J. E., "Wind Tunnel Experiments on the Flow over Rectangular Cavities at Subsonic and Transonic Speeds," Aeronautical Research Council, R&M 3438, London, Oct. 1964.

[14]Heller, H., and Bliss, D., "Aerodynamically Induced Pressure Oscillations in Cavities: Physical Mechanisms and Suppression Concepts," U.S. Air Force Fluid Dynamics Lab., AFFDL-TR-74-133, Dayton, OH, Feb. 1975.

[15]Rockwell, D., and Naudascher, E., "Review—Self Sustaining Oscillations of Flow Past Cavities," *Journal of Fluids Engineering*, Vol. 100, 1978, pp. 152–165.

[16]Hankey, W. L., and Shang, J. S., "Analysis of Pressure Oscillations in an Open Cavity," *AIAA Journal*, Vol. 18, No. 8, 1980, pp. 892–898.

[17]Rizzetta, D. P., "Numerical Simulation of Supersonic Flow over a Three-Dimensional Cavity," *AIAA Journal*, Vol. 26, No. 7, 1988, pp. 799–807.

[18]Tu, Y., "Unsteady Navier–Stokes Simulations of Supersonic Flow over a Three-Dimensional Cavity," AIAA Paper 92-2632, June 1992.

[19]Suhs, N. E., "Unsteady Computations for a Three-Dimensional Cavity With and Without an Acoustic Suppression Device," AIAA Paper 93-3402, Aug. 1993.

[20]Baysal, O., and Stallings, R. L., "Computational and Experimental Investigation of Cavity Flowfields," *AIAA Journal*, Vol. 26, No. 1, 1988, pp. 6, 7.

[21]Morgenstern, A., Jr., and Chokani, N., "Hypersonic Flow Past Open Cavities," *AIAA Journal*, Vol. 32, No. 12, 1994, pp. 2387–2393.

[22]Orkwis, P. D., Tam, C.-J., and Disimile, P. J., "Observations on Using Experimental Data as Boundary Conditions for Computations," *AIAA Journal*, Vol. 33, No. 1, 1995, pp. 176–178.

[23]Tam, C.-J., Orkwis, P. D., and Disimile, P. J., "Comparison of Baldwin–Lomax Turbulence Models for Two-Dimensional Open Cavity Computations," *AIAA Journal*, Vol. 34, No. 3, 1996, pp. 629–631.

[24]Ramakrishnan, S. V., Goldberg, U. C., and Ota, D. K., "Numerical Computation of Hypersonic Turbulent Flows Using Zero- and One-Equation Models," AIAA Paper 89-2234, July 1989.

[25]Gorski, J. J., Ota, D. K., and Chakravarthy, S. R., "Calculation of Three Dimensional Cavity Flow Fields," AIAA Paper 87-0117, Jan. 1987.

[26]Sarno, R. L., and Franke, M. E., "Suppression of Flow-Induced Pressure Oscillations in Cavities," *Journal of Aircraft*, Vol. 31, No. 1, 1994, pp. 90–96.

[27]Pereira, J. C. F., and Sousa, J. M. M., "Influence of Impingement Edge Geometry on Cavity Flow Oscillations," *AIAA Journal*, Vol. 32, No. 8, 1994, pp. 1737–1740.

[28]Baysal, O., Yen, G.-W., and Fouladi, K., "Navier–Stokes Computations of Cavity Aeroacoustics with Suppression Devices," *Journal of Vibration and Acoustics*, Vol. 116, Jan. 1994, pp. 105–112.

[29]Kim, I., and Chokani, N., "Navier–Stokes Study of Supersonic Cavity Flowfield with Passive Control," *Journal of Aircraft*, Vol. 29, No. 2, 1992, pp. 217–223.

[30]Jeng, Y.-N., and Payne, U.-J., "Numerical Study of a Supersonic Open Cavity Flow and Pressure Oscillation Control," *Journal of Aircraft*, Vol. 32, No. 2, 1995, pp. 363–369.

[31]Disimile, P. J., and Orkwis, P. D., "The Effect of Yaw Angle on the Dominant Frequencies of Rectangular Cavities in Supersonic Flow," Rept. 96-010, Dept. of Aerospace Engineering and Engineering Mechanics, Univ. of Cincinnati, OH, June 1996.

[32]Simpson, L. B., and Whitfield, D. L., "Flux Difference Split Algorithm for Unsteady Thin-Layer Navier–Stokes Solutions," *AIAA Journal*, Vol. 30, No. 4, 1992, pp. 914–922.

[33]Shang, J. S., and Hankey, W. L., Jr., "Numerical Solution for Supersonic Turbulent Flow over a Compression Ramp," *AIAA Journal*, Vol. 13, No. 10, 1975, pp. 1368–1374.

[34]Visbal, M., and Knight, D., "The Baldwin–Lomax Turbulence Model for Two-Dimensional Shock-Wave/Boundary-Layer Interactions," *AIAA Journal*, Vol. 22, No. 7, 1984, pp. 921–928.

[35]Degani, D., and Schiff, L. B., "Computation of Turbulent Supersonic Flows Around Pointed Bodies Having Crossflow Separation," *Journal of Computational Physics*, Vol. 66, No. 1, 1986, pp. 173–196.

[36]Praharaj, S. C., and Roger, R. P., "Effects of Interference Between a Missile and the Front Face of a Separated Booster," AIAA Paper 95-0332, Jan. 1995.

[37]Rockwell, D., and Knisely, C., "The Organized Nature of Flow Impingement Upon a Corner," *Journal of Fluid Mechanics*, Vol. 93, Pt. 3, 1970, pp. 413–432.

[38]Zhang, X., and Edward, J. A., "Computational Analysis of Unsteady Supersonic Cavity Flows Driven by Thick Shear Layers," *Aeronautical Journal*, Vol. 92, Nov. 1988, pp. 365–374.

Recommended Reading from Progress in Astronautics and Aeronautics

High-Speed Flight Propulsion Systems

S.N.B. Murthy and E.T. Curran, editors

This new text provides a cohesive treatment of the complex issues in high speed propulsion as well as introductions to the current capabilities for addressing several fundamental aspects of high-speed vehicle propulsion development. Nine chapters cover Energy Analysis of High-Speed Flight Systems; Turbulent Mixing in Supersonic Combustion Systems; Facility Requirements for Hypersonic Propulsion System Testing; and more. Includes more than 380 references, 290 figures and tables, and 185 equations.

1991, 537 pp, illus, Hardback
ISBN 1-56347-011-X
AIAA Members $54.95
Nonmembers $86.95
Order #: V-137 (830)

Place your order today! Call 1-800/682-AIAA

AIAA
American Institute of Aeronautics and Astronautics

Publications Customer Service, 9 Jay Gould Ct., P.O. Box 753, Waldorf, MD 20604
FAX 301/843-0159 Phone 1-800/682-2422 9 a.m. - 5 p.m. Eastern

Sales Tax: CA residents, 8.25%; DC, 6%. For shipping and handling add $4.75 for 1-4 books (call for rates for higher quantities). Orders under $100.00 must be prepaid. Foreign orders must be prepaid and include a $20.00 postal surcharge. Please allow 4 weeks for delivery. Prices are subject to change without notice. Returns will be accepted within 30 days. Non-U.S. residents are responsible for payment of any taxes required by their government.